Advances in the Analysis of Injection–Locked Oscillators

Almudena Suárez
Universidad de Cantabria
Santander, Spain
almudena.suarez@unican.es

Franco Ramírez
Universidad de Cantabria
Santander, Spain
ramirezf@unican.es

***Abstract*—This work reviews recent advances on the realistic analysis of injection–locked oscillators, for an efficient prediction of their complex multi–valued solution curves. The oscillator or its active core is modeled with a nonlinear admittance function extracted from harmonic balance, whereas other system elements are introduced at a second analysis stage. The analytical modeling of the external elements provides insight into their effect on the locking bands and other aspects of the behavior. In purely numerical simulations, the solution curves are traced through contour plots that make use of the nonlinear admittance function. The methods are illustrated with state–of–the–art applications, including compact transmitters and receivers, wireless–power transfer, and active sensing.**

Keywords—injection locking, harmonic balance, oscillator.

I. Introduction

The injection locking of oscillator circuits enables a variety of state–of–the–art applications in communication systems, wireless power transfer (WPT) and active sensing, among other. For instance, [1]–[2] proposes a Zero–IF self–oscillating mixer (SOM), based on an injection–locked oscillator, for compact and low–consumption transmitters and receivers. In near–field WPT systems, the use of a high–power oscillator [3] reduces the number of system elements and, thus, the total consumption. However, the oscillation frequency varies with the coupling conditions [4], which may lead to operation out of the allowed frequency band. This undesired frequency variation can be avoided through the injection locking of the power oscillator, as shown in [5]. As a third, and fully different application, active sensors based on injection locking [6] have recently been proposed. The sensing is based on the variation of the locking band with the material under test (MUT), which, as shown in [6], enables a high sensitivity with the advantage of a low phase noise.

Despite the interest of injection locking, predicting the solution curves of locked oscillators is involved. In this operation mode, the self–generated oscillation exhibits a time–constant phase shift with respect to the injection source, which is only possible in a certain frequency band [7]. For low input power there are three coexisting periodic solutions. Two solutions are oscillatory, each with a different phase shift (due to the sinusoidal dependences). They are respectively located in the upper and lower sections of an ellipsoidal curve, and only one of them is stable (physically observable). The third solution is not oscillatory; it can be seen as an evolution of the (trivial) dc solution of the free–running oscillator. In this kind of solution, the circuit responds to the input signal in a non–autonomous manner. By default, harmonic balance (HB) converges to the non–autonomous solution, so complementary methods are required. As the input power increases the behavior becomes more complex; the closed curve deviates from an ellipse and the non–autonomous one increases in amplitude, until they merge in a complex single curve with several points of infinite slope (turning points [7]).

The analysis of injection–locked oscillators often relies on an insightful model [8], based on a calculation/estimation of the oscillator quality factor. However, this model disregards the variation of the imaginary part of the oscillator immittance with the excitation amplitude and may not be accurate enough when dealing with transistor–based oscillators. On the other hand, HB simulations are involved due to the need to properly excite the self–oscillation and to the presence of multi–valued sections in the solution curves. Commercial HB generally fails to provide the locked solutions. In–house simulators make use of probes and continuation methods [9], but the analysis is not exhaustive, and can miss coexisting solution curves.

This work reviews three recently proposed analysis methods [5], [10], compatible with the use of commercial HB. In all cases, the oscillator or its active core is modeled with a nonlinear admittance function extracted from harmonic balance, whereas other system elements are introduced at a second analysis stage. The methods are illustrated through their application in compact transmitters and receivers, WPT and sensors.

II. Linearized Semi–Analytical Formulation

The first system considered is composed by two Zero–IF SOMs mutually locked by a wireless signal. One acts as a transmitter and the other as a receiver (Fig. 1). Each oscillator is described with its admittance function (Y_1 and Y_2) at the antenna connection node.

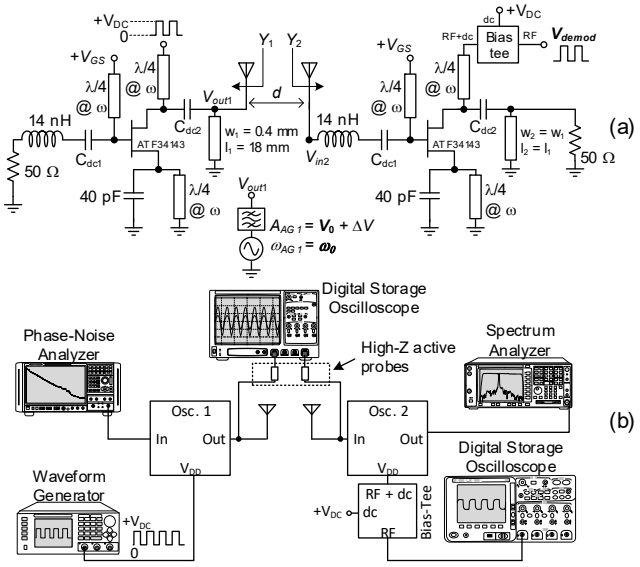

Fig. 1. System composed by two mutually locked Zero–IF SOMs. (a) Schematic. (b) Experimental setup.

Assuming a locked operation at the frequency ω, the system is formulated as:

$$\begin{aligned} Y_1(V_1,\omega,V_{DC})V_1 &= C(\omega)e^{-j\omega\tau}V_2e^{j\phi} \\ Y_2(V_2,\omega)V_2e^{j\phi} &= C(\omega)e^{-j\omega\tau}V_1 \end{aligned} \quad (1)$$

where V_{DC} is the bias voltage of the oscillator that acts as a transmitter, V_1 and V_2 are the respective voltage amplitudes, $\tau = d/c$ is the time delay, ϕ is the phase shift between the two oscillations and $C(\omega)$ is:

Work funded by the Spanish Ministry of Science and Innovation (MCIN/AEI/10.13039/501100011033) – PID2020-116569RB-C31.

$$C(\omega)=\frac{1}{R_{rad}}\sqrt{G_1G_2}\,\frac{c}{\omega d} \tag{2}$$

where G_1 and G_2 are the antenna gains, d, the distance, and R_{Rad}, the antenna resistance. If d is relatively large (the usual case), $C(\omega)$ will be small enough to enable the linearization of Y_1 and Y_2 about the standalone (uncoupled) solutions of the respective oscillators. Note that the functions on the right of (1) cannot be linearized in terms of ω due to their significant variation with d. Splitting (1) into real and imaginary parts:

$$\begin{aligned}
&Y^r_{1V}(V_1-V_{1o})+Y^r_{1\omega}(\omega-\omega_o)+Y^r_{1DC}(V_{DC}-V_{DCo})\\
&\qquad=C_1(\omega)\cos\left(\phi-\omega\tau\right)\\
&Y^i_{1V}(V_1-V_{1o})+Y^i_{1\omega}(\omega-\omega_o)+Y^i_{1DC}(V_{DC}-V_{DCo})\\
&\qquad=C_1(\omega)\sin\left(\phi-\omega\tau\right)\\
&Y^r_{2V}(V_2-V_{2o})+Y^r_{2\omega}(\omega-\omega_o)=C_2(\omega)\cos\left(\phi+\omega\tau\right)\\
&Y^i_{2V}(V_2-V_{2o})+Y^i_{2\omega}(\omega-\omega_o)=-C_2(\omega)\sin\left(\phi+\omega\tau\right)
\end{aligned} \tag{3}$$

where the superscripts indicate real and imaginary parts, the subscript "o" indicates standalone values (the standalone frequency ω_o is assumed identical), $C_1(\omega)=C(\omega)V_{o2}/V_{o1}$ and $C_2(\omega)=C(\omega)V_{o1}/V_{o2}$. Because the first oscillator acts as a transmitter and the second, as a receiver, in general we will have $C_1<<C_2$. The admittance derivatives are extraced from HB [10], using an AG (Fig. 1). This is separately introduced in each oscillator (in standalone operation) with the amplitude V_{om} (where $m=1,2$) and frequency ω_o. Thus, the original ratio between the AG current and amplitude is $Y_m=0$. The derivatives are calculated by applying finite differences to the AG amplitude and frequency, and to V_{DC}.

To obtain the locked solution curves versus V_{DC}, we first derive the relationship between ω and ϕ, by solving (3) for ω–ω_o. The resulting trascendental equation is addressed through a numerical procedure. Then, for each pair ω, ϕ, we solve (3) for V_{DC}–V_{DCo} and V_m–V_{mo}. The results (for different values of the common gain G and d) are shown in Fig. 2. The frequency basically follows the bias voltage V_{DC} of the transmitter oscillator. However, its variation is limited by the relationship $\omega(\phi)$. Note that ϕ is bounded (0 to 2π) and so is ω. Thus, the edges of the locking band depend on G and d. The amplitude in the transmitter oscillator is hardly affected by the mutual locking, due to the small C_1. Instead, the amplitude of the receiver oscillator exhibits the expected ellipsoidal variation [Fig. 2(b)].

The modulation signal is introduced in V_{DC}, and the modulated system is analyzed through an envelope–domain equation [10], derived from (1). Because the frequency increment due to the modulation is small, we perform a first–order Taylor series expansion C_1 and C_2 about each ω. The frequency increment $j\Omega$ gives rise to a time differentiation of the amplitudes and phases, which should be integrated in the envelope domain. Fig. 3 compares the transmitted baseband signal and the signal demodulated in second oscillator.

III. Nonlinear Semi–Analytical Formulation

We will consider a near field WPT system based on a Class–E oscillator (Fig. 4), which is injection–locked [5] to prevent its frequency variation with the coupling conditions. However, the locked–operation interval versus the coupling factor k wil depend on the values of the external–resonator elements. For an efficient selection, we will make use of a semi–analytical formulation. The locally introduced locking signal may be large enough to prevent the system linearization about the free–running solution. Thus, the oscillator active core will be described with a nonlinear admittance function. To extract this function, we introduce an AG in parallel at the coupled inductor node (Fig. 4). The locking source with the selected amplitude, E_g, is connected during this extraction. We perform a double sweep in the AG amplitude V and phase ϕ and calculate $Y_{AG}(V,\phi)$ as the ratio between the AG current and V. At each sweep step, we carry out a HB simulation with NH harmonics. However, the coupling effects will only be considered at the fundamental frequency, as enabled by the oscillator output filtering.

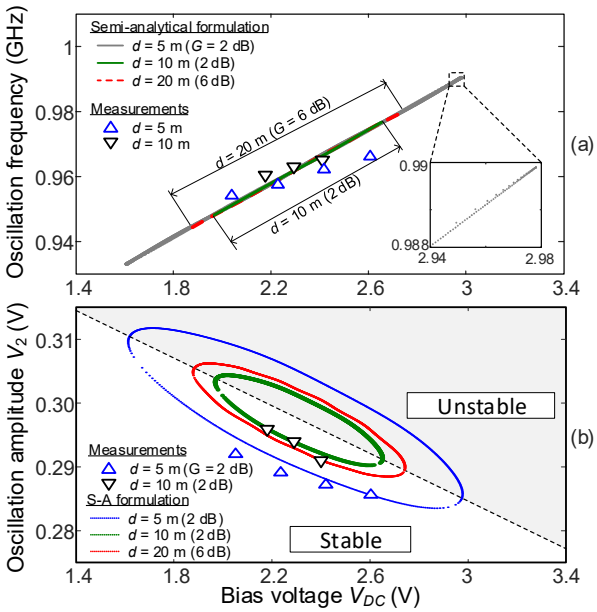

Fig. 2. Solutions of the mutually locked system under different G and d values, traced versus V_{DC}. (a) Oscillation frequency. (b) Amplitude in the receiver oscillator.

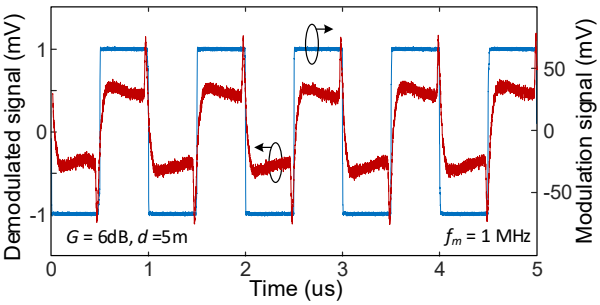

Fig. 3. Demodulation of a rectangular signal at 1 MHz.

Assuming a locked operation, the system is described with:

$$\begin{aligned}
&Y^r_{AG}(V,\phi)+\frac{R_2k^2}{\left[(1-k^2)^2+2\gamma^{-1}(k^2-1)+\gamma^{-2}\right](L\omega)^2+R_2^2}=0\\
&Y^i_{AG}(V,\phi)+\frac{1}{L\omega}\\
&\quad-\frac{1}{L\omega}\left(\frac{R_2^2+\left[(1-k^2)+\gamma^{-1}(k^2-2)+\gamma^{-2}\right](L\omega)^2}{\left[(1-k^2)^2+2\gamma^{-1}(k^2-1)+\gamma^{-2}\right](L\omega)^2+R_2^2}\right)=0
\end{aligned} \tag{4}$$

where $\gamma=LC\omega^2$. The function $Y_{AG}(V,\phi)$ is extracted in the presence of the inductor, so one must subtract its reactance. As gathered from (4), the detuning γ, will have a significant impact on the locked–operation intervals versus k [5]. To

obtain the solution curve, we sweep k and, at each k step, we calculate V and ω from the intersections of the two curves in (4) in the plane (ω, V). The variation of the drain efficiency for P_{in} = –0.45 dBm is shown in Fig. 5. For γ = 0.82 and γ = 1.23 there are two disconnected curves, and the locked operation interval is delimited by a turning point in the high–amplitude curve. For γ =1.03 the curves are merged, which leads to a large interval of locked operation. With this semi–analytical method, the solution curves are traced in a fast manner, with no need for convergence procedures. This enables an efficient selection of the resonator elements. Full HB results (with more demanding simulations) are overlapped [5]. Measurements are superimposed in Fig. 5.

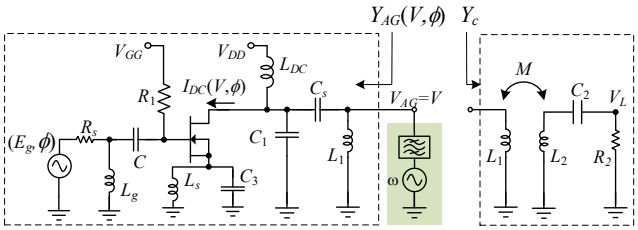

Fig. 4. Injection–locked Class–E oscillator. Extraction of $Y_{AG}(V,\phi)$ from HB simulations and coupled network, described with the admittance Y_c.

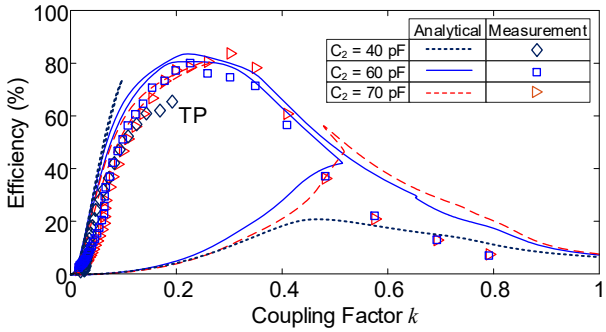

Fig. 5. Solution curves of for different γ values. Measurements are superimposed.

IV. Contour Method

The third method, purely numerical, will be illustrated through its application to an injection–locked sensor. It can be implemented on commercial HB through the introduction of specific functions [5]. The oscillator contains a distributed LC resonator connected to its gate terminal (Fig. 6), as well as a locking source introduced at the same node. The aim is to analyze the variations of the locking band with the dielectric constant ε_r of the MUT, placed over the capacitive section of the resonator. Now, the nonlinear admittance function will account for the full oscillator, in the absence of the input source. For each ε_r, we will carry out a double sweep in the amplitude V and frequency ω of an AG (connected to the gate node) and perform an HB simulation with 5 harmonics at each sweep step. This will provide the function $Y_{AG}(\varepsilon_r, V, \omega)$. The solution curve under the input current I_g is obtained by tracing the following contour in the plane (V, ω):

$$\left|Y_{AG}(\varepsilon_r,V,\omega)\right|\left|V\right| = I_g \qquad (5)$$

Note that the input source is not present during the extraction of $Y_{AG}(\varepsilon_r, V, \omega)$. The family of solution curves obtained for I_g = 5 mA is shown in Fig. 7. It demonstrates the impact of ε_r on the locking band. The curves have been validated through a demanding AG optimization [5] (using 5 harmonics) with overlapped results. As a key advantage, (5) provides the whole family of solution curves versus I_g through simple contour plots, with no need to re–simulate the circuit.

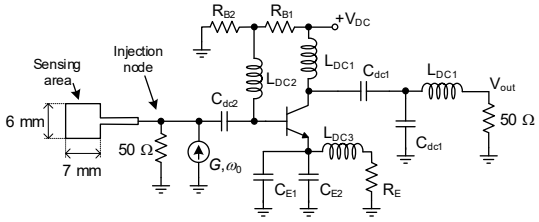

Fig. 6. Schematic of the sensing oscillator. The material under test is placed over the capacitive section of the distributed resonator.

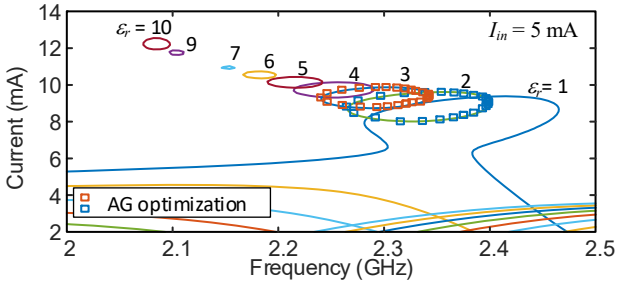

Fig. 7. Variation of the locked solution curves with the dielectric constant.

Conclusions

New methods for the analysis and optimized design of injection–locked oscillators have been presented. The oscillator or its active core is modeled with functions extracted from harmonic balance, whereas the external elements may be described in an analytical manner. The methods, semi–analytical and purely numerical, enable a realistic and efficient prediction of the complex multi–valued curves intrinsic to this mode of operation.

References

[1] P. Burasa, N. G. Constantin, K. Wu, "Low-power injection-locked Zero-IF self-oscillating mixer for high Gbit/s data-rate battery-free active µRFID tag at millimeter-wave frequencies in 65-nm CMOS," *IEEE Trans. Microw. Theory Techn.*, vol. 64, no. 4, pp. 1055-1065, 2016.

[2] P. Burasa, B. Mnasri, K. Wu, "Millimeter–Wave CMOS Sourceless Receiver Architecture for 5G–Served Ultra–Low–Power Sensing and Communication Systems,2 *IEEE Trans Microw. Theory Techn.*, vol. 67, no. 5, pp. 1688–1696, May 2019.

[3] A. Costanzo, M. Dionigi, F. Mastri, M. Mongiardo, "Rigorous modeling of mid–range wireless power transfer systems based on royer oscillators*," 2013 IEEE Wirel. Power Transf. WPT 2013*, pp. 69–72.

[4] V. Ardila, F. Ramirez, A. Suarez, "Nonlinear Dynamics of an Oscillator Inductively Coupled to an External Resonator for Power Transfer and Data Transmission," *IEEE Trans. Microw. Theory Techn.*, vol. 70, no. 4, pp. 2418–2431, Apr. 2022.

[5] V. Ardila, F. Ramírez, A. Suárez, "Analysis and Design of Injection–Locked Oscillators Coupled to an External Resonator," *IEEE Trans. Microw. Theory Techn.*, vol. 71. DOI**:** 10.1109/TMTT.2023.3259223

[6] R. Mirzavand, M. M. Honari, P. Mousavi, "High–Resolution Dielectric Sensor Based on Injection–Locked Oscillators," *IEEE Sensors J.*, vol. 18, no. 1, pp. 141–148, 1 Jan.1, 2018.

[7] J. Guckenheimer and P. J. Holmes, *Nonlinear Oscillations, Dynamical Systems, and Bifurcations of Vector Fields*, vol. 42. 1983.

[8] R.A. Adler, "A study of locking phenomena in oscillators," *Proc. IEEE,* 61, 1380–1385, 1973.

[9] M. Pontón, S. Sancho, A. Herrera, A. Suárez, "Wireless Injection Locking of Zero–IF Self–Oscillating Mixers," *IEEE Trans. Microw. Theory Techn.*, vol. 70, no. 1, pp. 836–849, Jan., 2022.

[10] S. Sancho, F. Ramírez, M. Pontón, A. Suárez, "Analysis of a Sensor Based on an Injection–Locked Oscillator Driven by a Chirp Signal," *2023 IEEE MTT–S Int. Microwave Symp.*, San Diego, CA, USA, June.